

Synthesis and performance evaluation of olive fruit waste resin for removal of fluoride from aqueous solution: batch and column modeling

Raid Alrowais^a, M.T. Bashir^{a,b,*}, Muhammad Ali Sikandar^b, Mohsin Ali Khan^{b,c}

^aDepartment of Civil Engineering, Jouf University, Al-Jawf, Saudi Arabia, emails: tariqbashir@cecos.edu.pk (M.T. Bashir), rnalrowais@ju.edu.sa (R. Alrowais)

^bDepartment of Civil Engineering, CECOS University of IT and Emerging Sciences, Peshawar, Pakistan, email: msikandar@cecos.edu.pk (M.A. Sikandar)

^cDepartment of Structural Engineering, Military College of Engineering (MCE), National University of Science and Technology (NUST), Islamabad, Pakistan, emails: mohsin.ali@cecos.edu.pk/moak.pg18mce@student.nust.edu.pk (M.A. Khan)

Received 17 September 2021; Accepted 30 January 2022

ABSTRACT

The excessiveness of fluoride in water triggers severe environmental problems and adversely affects human health. This research is focused on the preparation of novel adsorbent through modification of olive fruit waste (OFW) characteristics via hydroxyl radical pre-treatment and quaternization for fluoride adsorption. A remarkable removal performance was achieved with pH ranging between 3 and 9. The highest adsorption capability of quaternized olive fruit waste-based adsorbent could reach 2.35 mg g⁻¹ at pH equalling 6 and 2.01 mg g⁻¹ at neutral pH. The overall size of the anion exchange resin ranging between 0.25 and 0.5 mm was vital in the biosorption mechanism, providing the removal performance up to 5.15 mg g⁻¹ in column study. The performance was evaluated employing the models including Langmuir isotherm and pseudo-second-order model as well as Thomas and Adams–Bohart models. Langmuir isotherm ($R^2 = 0.985$) and pseudo-second-order model ($R^2 = 0.999$) provide better results than Freundlich isotherms and pseudo-first-order models, respectively. The scanning electron microscopy revealed significant variability in morphology with projections and porous surfaces, which were confirmed by Brunauer–Emmett–Teller assessment. Fourier-transform infrared spectroscopy and CHNS analysis also verified the existence of amine group and hydroxyl ions on bio-adsorbent and active points. The outcomes of this research advocate that the OFW based adsorbent have a notable prospect in engineering application.

Keywords: Adsorption; Thomas modelling; Fluoride; Mercerization; Quaternization

1. Introduction

Fluoride intrusion in drinkable water is directly linked to a number of negative health effects, including neurological problems, bone weakening, and ossification of ligaments and tendons [1–3]. One of the major contributors to the excessiveness of fluoride content in groundwater is the suspension of fluoride-rich minerals, including the discharge of fluoride-containing agricultural and agricultural effluents

including petrochemical, semiconductor, and mining industries could lead to harmful water pollution [2,4]. Despite the fact that the World Health Organization (WHO) recommends a fluoride content in drinkable water guideline of 0.5–1.5 mg L⁻¹, more than 250 million people are nevertheless exposed to fluoride-contaminated water [2,3].

Adsorption is one of the most promising techniques for effectively removing the excess fluoride in water due to its low manufacturing cost and ease of usage [5,6]. The

* Corresponding author.

adsorption encompasses a physicochemical method for water purification in which chemical or physical forces drive the water-soluble molecules for attachment onto the adsorbent surface. Adequate technique for selecting adsorption process has a significant impact on treatment efficiency [7]. In particular, the utilization of agricultural waste with economical chemical treatment has attracted researchers in the past few decades. Moreover, ion-exchange resins (IERS) can be used for several purposes, including the desalination of seawater, removal of fluoride and nitrates, hard water softening, metal ion recovery, lake purification, as well as purification of water and different products [1,8,9]. Various adsorbents reliant on zeolite and other materials, including activated alumina, have been created for fluoride extraction. However, most of these produced adsorbents have adsorption capacity, pH range, and mechanical strength limitations [5,6].

Due to its superior binding capacity and variety of source materials, biomaterials, particularly those based on inactive agriculture wastes, have recently attracted a lot of study awareness for uptake of ionic pollutants [10]. Hazardous reagents can be avoided by synthesizing the biomaterial-based ion-exchange resins by a chemical treatment called mercerization followed by quaternization [4,8]. Olive fruit waste (OFW) is available in abundance in many regions of the world, including the Aljouf region of Saudi Arabia, that can be transformed into effective anion exchangers for water purification, including fluoride to avoid ill effects [11]. Ezzeldin et al. [8] developed anion exchangers with superior properties to commercial anion exchange beads made from olive oil waste (OW) through chemical treatment. Adsorbents made from agricultural wastes employing chemical procedures are cost-effective and environmental-friendly. This can be achieved by grafting lignocellulosic agricultural wastes with amine groups to produce a large number of anion exchangers [2]. Inserting a range of

agricultural wastes, including rice husk, sawdust, sugarcane bagasse, pine bark, coconut husk, *Moringa oleifera* hull, and persimmon tea leaf, can be used to convert agro-waste into an anion exchanger [12–14]. Orlando et al. [12] used pyridine as a catalyst in a chain reaction of epichlorohydrin and dimethylamine to create an exchange (EDM method). Wheat straw-based anion exchangers were also created by Bashir et al. [2], Koay et al. [15], and Xing et al. [16] for efficient elimination of anions from an aqueous solution.

OFW can also be attuned to improving its attraction for anions elimination. OFW is an agricultural waste produced during the processing of olives that contains adequate lignocellulosic content, and it can be used as a novel precursor by chemical treatment to make lignocellulose-based anion resins. Hence, the study objective concentrated on the lignocellulosic content of OFW, batch capacity, kinetic behaviour, and its subsequent fitness for anions elimination such as fluoride. It also focused on in-depth column study and modeling to observe the commercial viability of this novel adsorbent.

2. Materials and methodology

Olive fruit and agricultural waste were employed as precursors for the adsorbent preparation. Fig. 1 demonstrates a methodological flow diagram illustrating numerous elements in this research.

2.1. Material and solution preparation

The analytical grade reagents with purity $\geq 99\%$, including NaF, KOH, NaOH, and acetic acid, were obtained from Sigma-Aldrich without additional purification. 2.21 g NaF was dissolved in 1 L deionized (DI) water to make $1,000 \text{ mg L}^{-1}$ fluoride stock solution. The necessary concentrations of

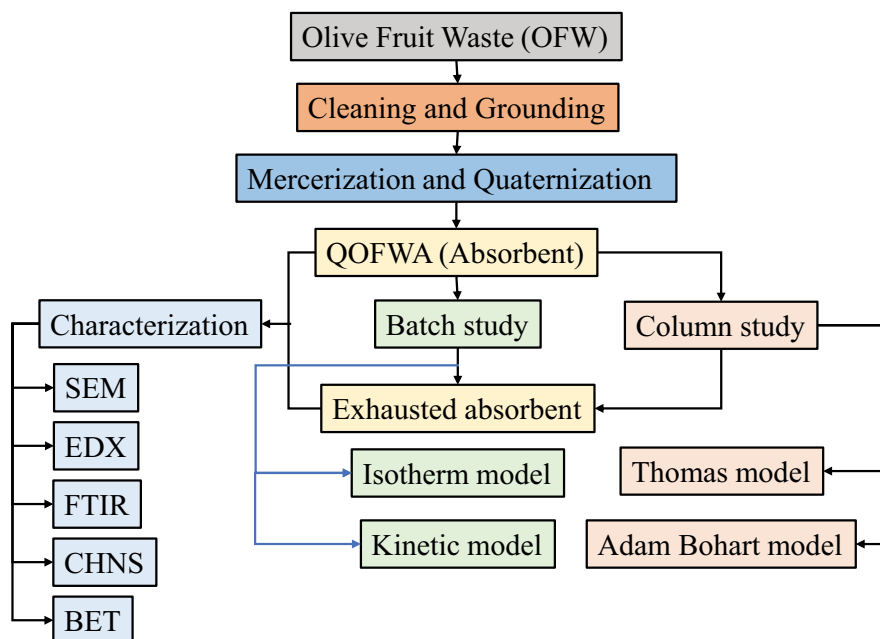


Fig. 1. Methodological flow diagram of current research work.

solutions utilized in this research were produced via dilution of fluoride stock solution and DI water. Using a micro-pipette, a number of specimens were produced with ultimate concentrations ranging between 2.5 and 15 mg L⁻¹ having a gradual increment of 2.5 mg L⁻¹. SPADES is a commonly employed technique to determine fluoride in waters by taking into account the absorbance of the fluoride ion. Hence, the SPADES technique with DR/2500 Spectrophotometer (Hach) was used to verify final concentrations.

2.1.1. Adsorbent preparation

OFW was acquired from the local industry of Sakaka, Aljouf, Saudi Arabia. After washing, 1 kg of raw OFW with hot tap water was then oven-dried before its treatment with concentrated H₂SO₄ for 24 h. Further preparation of adsorbent was conducted using the method by Bashir et al. [6] with slight modifications. The obtained OFW particles were rinsed with DI water before neutralizing to pH 7 with NaOH. Again, after drying, they were grounded to small particle sizes ranging between 0.25 and 2 mm. To guarantee the complete elimination of extrinsic water activity, the drying procedure was completed at 105°C. The OFW was then mercerized in KOH solution (30%) for approximately 2 h at room temperature to cause the particles to swell. Researchers conclude that NaOH expanded the biomaterial, including cotton yarn fibers, resulting in variation of chemical composition [17,18]. The resultant mercerized OFW was washed using distilled water before immersed in acetic acid (5%) and drying at 60°C.

Following mercerisation and drying, quaternization was carried out in units holding 40 g of mercerized OFW. At 70°C for 18–20 h duration, the mercerized OFW was subjected to react in a 500 mL solution containing 60% N-(3-chloro-2-hydroxypropyl) trimethylammonium chloride (CHMAC) and 5 M KOH and in the proportion 1.5:1.0 (v/v). This procedure generated additional positive charges on resins by bonding amine groups amid alkaline environments. While mixing, the resins of quaternized olive-fruit-waste-based adsorbent (QOFWA) were continuously washed with the appropriate amount of deionized water. The pH of the solution was regulated by 1 M NaOH and 1 M HCl after getting a clear precipitate. Each QOFWA batch was dried at 105°C before being distributed in resin of size ranges: 0.25–0.5 mm, 0.5–1 mm, and 1–2 mm.

2.2. Characterization of adsorbent

2.2.1. Determination of point of zero charge and zeta potential

The procedure of the pH drift method was followed to compute the point of zero charge (pH_{PZC}). The suspension of QOFWA dosage in 0.01 M NaNO₃ for the duration of 24 h changes the pH significantly. The pH of a 50 mL solution can then be modified either using NaOH or HNO₃ solution. The initial pH was determined after 60 min of stirring to attain equilibrium, and 1.5 g of NaNO₃ was supplied to every solution to reach the ultimate electrolyte concentration of about 0.45 M. The ultimate pH was determined after another 3 h. When the data were plotted as a change in pH vs. final pH, the point of zero change in pH was calculated.

Zeta potential was determined by preparing the suspensions of QOFWA in 0.01 M NaCl solution in the pH range between 3 and 10 employing the method described by Bashir [14]. The sample solution was agitated in the incubator shaker for a period of 2 h. Subsequently, a fractional amount of filtrate from each sample was collected to observe zeta potential, followed by measuring zeta potential using Zetasizer (Malvern, UK).

2.2.2. Scanning electron microscopy and energy dispersive X-ray spectroscopy

The scanning electron microscopy (SEM) was utilized to access the surface morphology of QOFWA (JEQ, Japan) by coating the surface of the samples with a thin platinum film for electric conductivity. While for elemental analysis, and energy dispersive X-ray spectrophotometer abbreviated as energy dispersive X-ray spectroscopy (EDX) (JED 2300) was utilized.

2.2.3. Fourier-transform infrared spectroscopy

The occurrence of various classes and patterns on QOFWA and fluoride-loaded QOFWA was determined using Fourier-transform infrared (FT-IR) examination (1750X, Perkin Elmer). FT-IR is an excellent method for identifying the functional groups on the surface of QOFWA and drained QOFWA after utilization. The spectra were taken between 400 and 4,000 cm⁻¹ and then automatically analyzed using the spectrum program included with the device.

2.2.4. Brunauer–Emmett–Teller surface area

Highly precise, fully automated gas sorption equipment (Gemini Analyzer, Micrometric USA) was utilized to estimate surface area and the pore volume of the QOFWA. QOFWA was vacuumed for 4 h at 150°C with a target to eliminate accumulated gases and any traceable moisture from the product. This procedure was carried out prior to the adsorption–desorption of nitrogen gas at 77 K. Furthermore, using the designed software in the instrument, Brunauer–Emmett–Teller (BET) was exploited to compute pore volume and surface area. While the Barrett, Joyner, and Halenda (BJH) model was operated in the program to estimate the pore size distribution.

2.2.5. Elemental composition of OFW and QOFWA

An elemental analyzer (Perkin Elmer – Series II 2400, Japan) was used to evaluate the OFW and QOFWA for hydrogen, nitrogen, carbon, and sulfur elements. The QOFWA has a wide range of chemical characteristics and qualities, including cellulosic components with plentiful carbon and adequate nitrogen, which can be successfully used in the development of a successful anion-based sorbent.

2.3. Fluoride batch study

Batch research was carried out to determine the fundamental parameters, including pH, contact duration, initial fluoride concentration for specified dosage of QOFWA

followed by adsorption capacity. The initial fluoride concentration and pH ranging between 2.5–15 mg L⁻¹, 3–9, and 0.1–0.6 g, respectively, were all found. The parameters were defined using a fluoride concentration of 5 mg L⁻¹ considering the presence of fluoride in groundwater sources at this quantity [2]. The results of these experiments also aided in the investigation of Langmuir and Freundlich isotherm models, as well as kinetic models such as pseudo-first and second-order models along with column modeling, including the Thomas and the Adams–Bohart models. Batch tests were performed by putting 100 mL of sample in 250 mL Erlenmeyer flasks and mixing at 28°C with a 2°C precision. To reduce error, each test was repeated three times.

2.4. Isotherm modelling for fluoride adsorption

To examine the applicability and performance of adsorption, the linearized version of two isotherms, namely Langmuir isotherm [Eqs. (1)–(3)] and Freundlich isotherm models [Eq. (4)], are employed [6,19].

$$q_e = \frac{Q_0 \cdot b \cdot C_e}{1 + b \cdot C_e} \quad (1)$$

$$\frac{1}{q_e} = \frac{1}{Q_0 \cdot b \cdot C_e} + \frac{1}{Q_0} \quad (2)$$

$$R_L = \frac{1}{1 + K_L \cdot C_e} \quad (3)$$

$$\log \frac{x}{m} = \frac{\log K_f + 1}{n \log C_e} \quad (4)$$

where Q_0 the maximal monolayer ability in mg g⁻¹, q_e the quantity of solute adsorbed in mg g⁻¹, C_e denotes the equilibrium concentration in mg L⁻¹, and m denoting the mass of adsorbent utilized in g. While b and R_L are the Langmuir isotherm constant and separation factor, respectively. In the Freundlich model, $1/n$ and coefficients K_f represent the adsorbent intensity and capacity, respectively.

2.5. Kinetic modeling

Adsorption kinetics models, namely pseudo-first and second-order models, were employed to understand better the process of fluoride uptake kinetics using the waste material. For the pseudo-first-order model, the Lagergren equation [Eq. (5)] was incorporated, while second-order model behaviour was investigated by employing Eq. (6) [20,21].

$$\ln(q_e - q_t) = \ln q_e - k_1 t \quad (5)$$

$$\frac{t}{q_t} = \frac{1}{K_2 q_e^2} + \frac{1}{q_e} t \quad (6)$$

where q_t represents the amount of fluoride absorbed in mg g⁻¹ at time t , and q_e is the quantity of fluoride absorbed

at equilibrium in mg g⁻¹. The constants are K_1 (min⁻¹) and K_2 (g mg⁻¹ min⁻¹), reflecting the kinetic rate of pseudo-first and second-order models, respectively. Moreover, R^2 factor is traditionally employed to conclude the best fit of the model, but it does not reflect errors in the curve [22]. To overcome this limitation, residual root mean square error (RMSE) is calculated to observe fitting of the curve as lower is RMSE value, better will be the fitting [22].

2.6. Column modeling

To compute the required parameters for Thomas and Adams–Bohart models, the examined data from all tests performed in continuous flow columns design was employed.

2.6.1. Thomas model

In many cases, the Thomas model is utilized to assess column efficiency [23,24]. Adsorbate maximal solid-phase concentration on adsorbent can be computed using the continuous flow column data. Since the Thomas model considers the adsorption rate constant operating the kinetic data to calculate it [25,26]. To remove fluoride on QOFWA, this model is used to fit the data collected. Time against $\ln(C_i/C_t - 1)$ was used to determine R^2 , intercept and slope for the Thomas model using excel spreadsheets. Eq. (7) was used to compute the Thomas adsorption capacity (q_{th}) in mg g⁻¹. Thomas constant (k_{th}) in L mg⁻¹ min⁻¹. While Eq. (8) shows the linearized form of the Thomas model.

$$\frac{C_t}{C_i} = \frac{1}{1 + e^{\left(\frac{k_{th} q_{th} m}{v} - k_{th} C_i t\right)}} \quad (7)$$

$$\ln\left(\frac{C_t}{C_i} - 1\right) = \frac{k_{th} q_{th} m}{v} - k_{th} C_i t \quad (8)$$

where “ m ” is the mass of the adsorbent in (g), and “ v ” is the flow rate in (mL min⁻¹). In nonlinear regression analysis, the kinetic coefficient “ k_{th} ” (L mg⁻¹ min⁻¹) and adsorption capacity of the column “ q_{th} ” (mg g⁻¹) can be calculated by drawing a curve or using excel spreadsheets to analyze $\ln(C_i/C_t - 1)$ against time “ t ”.

2.6.1. Adams–Bohart model

Adams–Bohart model parameters were calculated based on the observed data for fixed beds. Time and $\ln(C_i/C_t)$ were used to determine the parameters such as intercept, slope, and R^2 . Eq. (9) was used to obtain the rate constant “ K_{ab} ” (L mg⁻¹ min⁻¹) and the saturation concentration “ N_0 ” (mg L⁻¹).

$$\ln\left(\frac{C_t}{C_i}\right) = k_{ab} C_i t - k_{ab} N_0 \frac{Z}{V_L} \quad (9)$$

There are several variables considered, that is, “ K_{ab} ”: Adams–Bohart kinetic constant (mg L⁻¹), “ N_0 ”: saturation concentration (mg L⁻¹), “ Z ”: depth of bed (cm), “ V_L ”: linear velocity (cm s⁻¹) which is equal to flow divided by

cross-sectional area of the column. “ N_0 ” and “ K_{ab} ” can be computed by drawing a plot between $\ln(C_i/C_0)$ and time, taking advantage of excel spreadsheets with the appropriate parameters.

3. Results and discussion

3.1. Surface charge of QOFWA

3.1.1. Point of zero charge (pH_{PZC}) of QOFWA

The pH_{PZC} made it conceivable tending it to attribute the physical characteristic of an adsorbent for its efficacy in a specific pH range. As described in detail in the section on the change in pH, pH_{PZC} was determined by considering the starting and final pH values, and a graph (Fig. 2) was generated between the initial pH values and their respective change in pH values. It can be seen that the intersection of the line plot with the x-axis representing zero change in pH value is equal to 7.7. The resulting value lies in the range $2-8 \pm 0.2$, depicting the positive surface charge density on QOFWA. Therefore, QOFWA aided in developing favorable conditions for anions such as fluoride adsorption.

3.1.2. Zeta potential of QOFWA

In the current research study, the QOFWA based adsorbent used for the removal of fluoride was prepared using a novel technique. It can be seen in Fig. 3 that the final results of zeta potential lie in the range between 29.5 and 23.6 mV. Till pH equaling around 7.19, the QOFWA maintained an isoelectric point in the positive region or positive charge due to protonation of amine groups occurring at pH fewer than 7.19. An additional rise in pH induced deprotonation, which resulted in driving the isoelectric points in the negative region. Furthermore, Fig. 3 also shows that the positive charge increases over a wider pH range depicting the concentration of functional groups in QOFWA. The drop in the measured zeta potential with an increase in pH from 3

to 10 might be due to the hydroxyl and carboxyl groups on QOFWA. Thus, resulting in a lower positive charge at elevated pH. By Van der Waals interactions, the anions elimination such as fluoride can be significantly increased to a pH of 7.19. Xing et al. [16] noticed an analogous trajectory in eliminating heavy metals (nitrate and phosphorous) using the agro-based ion exchangers like wheat stalk and wheat straw produced via chemical treatment.

3.2. Surface and chemical analysis of OFW and QOFWA

The surface morphology and pores found in OFW and QOFWA were observed adopting SEM at 5 kV at a resolution ranging from 1,000X to 1 K. The SEM depictions showed significant changes in surface structure, and QOFWA achieved projections with smooth surfaces, pores, and cracks. Fig. 4A–C illustrate the image of raw OFW, QOFWA, and fluoride-loaded QOFWA with EDX spectra (Fig. 4D), respectively. The existence of adsorbed fluoride was verified by quantitative assessment using EDX.

Furthermore, FT-IR analysis of OFW and QOFWA revealed that QOFWA possesses substantial variations. Many different frequencies are projected in QOFWA, which were disappeared in the raw OFW, as can be seen in Fig. 5A and 5B. Furthermore, FT-IR revealed the existence of amine and hydroxyl groups inside the QOFWA as a result of CHMAC grafting, indicating suitable scenarios for fluoride adsorption. For example, in a wide range of stretches between $3,400$ and $3,800\text{ cm}^{-1}$, the dominance of the hydroxyl group was observed. Furthermore, the N–H stretch, which reflected primary aliphatic amines, was given $3,404\text{ cm}^{-1}$. Compared to QOFWA, the OFW spectra showed a weak unique pattern of bands ranging from $2,900$ to $1,700\text{ cm}^{-1}$ related only to the aromatic rings found in the lignin polymeric chain structure. The spike at 900 cm^{-1} in the QOFWA spectra, ascribed to the C–N stretch, was absent in the OFW spectral range. Furthermore, the spike at $1,422\text{ cm}^{-1}$ upon QOFWA is attributed to the C–H stretch of tert-butyl groups from

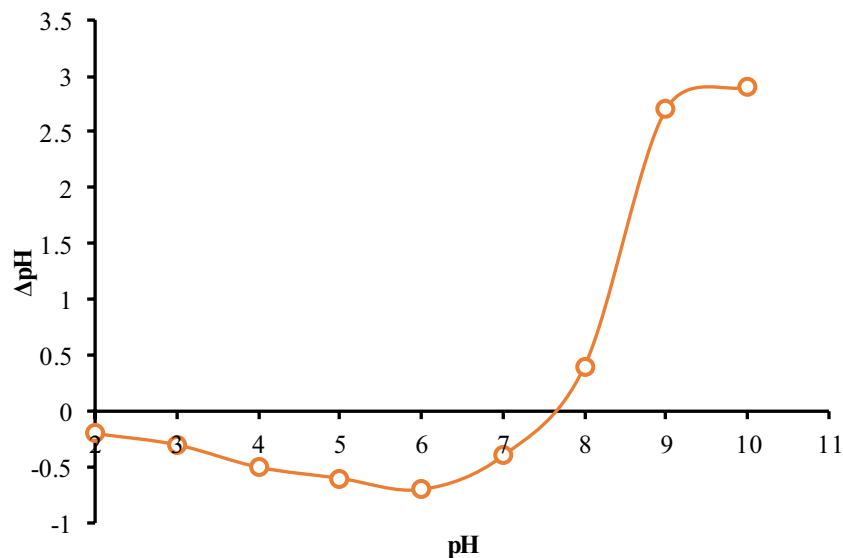


Fig. 2. Variation of ΔpH with pH for observing point of zero charge on QOFWA (dosage: 4 g L^{-1} ; temperature: 28°C).

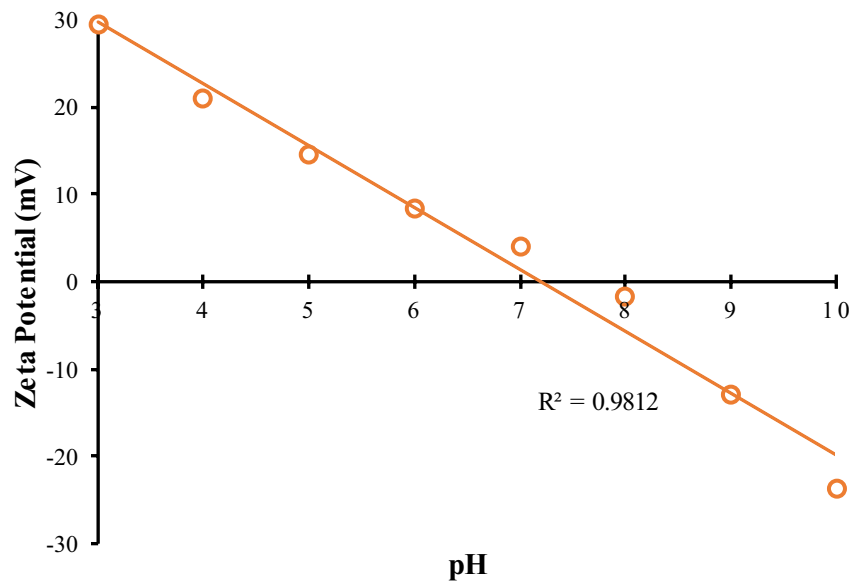


Fig. 3. pH vs. zeta potential plot for QOFWA (dosage: 4 g L⁻¹; temperature: 28°C).

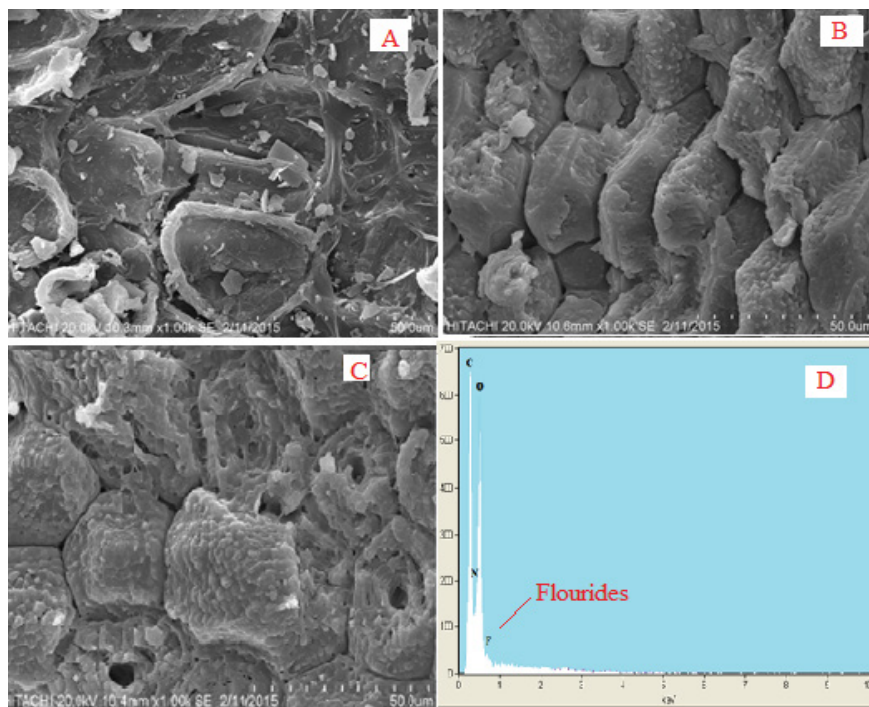


Fig. 4. Scanning electron microscopy images (A) raw OFW, (B) QOFWAA, (C) fluoride loaded QOFWAA, and (D) EDX spectrum of fluoride loaded QOFWAA.

CHMAC. For OFW and QOFWA, the strengthening phase of C–O in C–O–C glycosidic links occurred at 1,045 and 1,047 cm⁻¹, respectively.

3.3. BET surface area of the OFW and QOFWA

The BET surface area, diameter, width, and mean volume of pores were all determined. BJH was employed to calculate the width and volume of pores using the designed

software package in the device. The BET isotherm for desorption and adsorption of particles with sizes 0.125–0.25 mm and 0.25–0.5 mm indicated macro and mesopores, respectively, on the surface of QOFWA. The existence of a large volume of macro and mesopores in the adsorbent makes it an excellent match for pollutant and toxin adsorption in water, allowing pollutants to enter [27]. The maximum size of fluorine (0.27 mm) further confirms the stated phenomena [13]. Additionally, Table 1 dictates that the BET

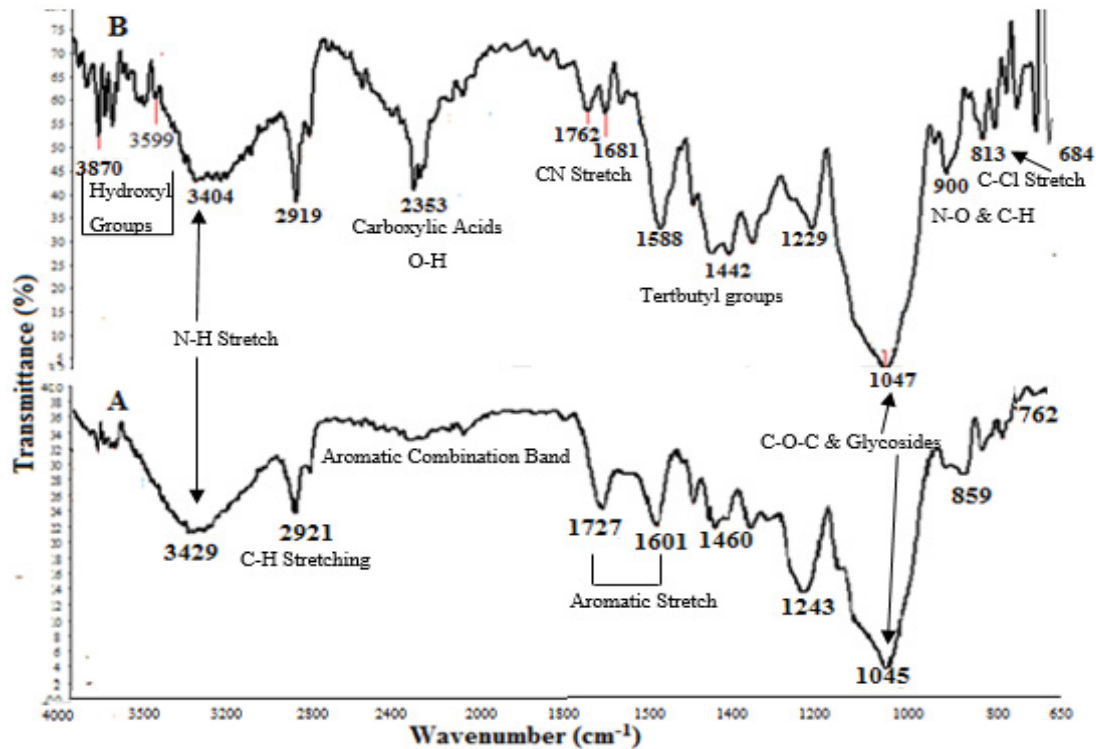


Fig. 5. FT-IR spectrums for (A) raw OFW and (B) QOFWA.

Table 1

Observation of BET surface area, pore volume, and diameter volume of raw OFW and QOFWA

Description	Size (mm)	BET area ($\text{m}^2 \text{g}^{-1}$)	Pore size (nm)	Mesopore d_{Av} ($2 < d < 50 \text{ nm}$)	Macropore d_{Av} ($d > 50 \text{ nm}$)	Pore V_{Av} ($\text{cm}^3 \text{g}^{-1}$)
OFW	0.125–0.25	0.72	12.509	12.55	80.21	8.02×10^{-4}
QOFWA _S	0.125–0.25	1.39	13.467	9.06	95.51	8.84×10^{-4}
QOFWA _M	0.25–0.50	0.85	39.332	21.35	115.82	18.30×10^{-4}
QOFWA _L	0.50–1.00	0.44	60.176	48.73	115.96	15.49×10^{-4}

QOFWA_S = QOFWA (Small); QOFWA_M = QOFWA (Medium); QOFWA_L = QOFWA (Large)

surface area of QOFWA for particle sizes of 0.125–0.25 and 0.25–0.5 mm is enhanced by 48.2% ($1.39 \text{ m}^2 \text{g}^{-1}$) and 15.3% ($0.85 \text{ m}^2 \text{g}^{-1}$), respectively. While, the BJH adsorption indicates that the improved average size of pores for QOFWA providing values of 13.47, 39.33, and 60.18 nm for particle sizes 0.125–0.25, 0.25–0.5, and 0.5–1 mm, respectively.

3.4. CHNS-elemental analysis of OFW and QOFWA

Table 2 shows the findings of CHNS studies on OFW, QOFWA, and fluoride-loaded QOFWA. The nitrogen concentration in OFW and QOFWA was found to be 3.28% and 3.51% by weight, respectively. The treatment of mercerized OFW using CHMAC raised the nitrogen content of QOFWA from 3.28% to 3.58%, that is, 8.38% by weight increase. This increment in the quantity of nitrogen may be due to nitrogen partitioning or absorption on the external sphere complexation, as well as loading within the pores [28]. Mokaloba

and Batane [29] showed in their research that chemical treatment, that is, mercerization of OFW using KOH, particularly on wooden products, strengthened the cell structure of cellulose and enhanced the dimensional stability. Furthermore, the reaction rate of acetylated and mercerized cellulose is considerably faster and more effective than that of succeeding compounds [7,30]. Hence, these results supported the claim that mercerization treatment using KOH improved the effectiveness of QOFWA.

3.4.1. Effect of pH

The pH ranging between 3.0 and 9.0 was used to investigate the impact of pH on fluoride elimination. Fluoride elimination via bio-adsorbent is strongly reliant on the aqueous phase of pH. [31,32]. Biomacromolecules like thiol, amino, carboxyl, and phenol groups are found in bio-adsorbents based on biomass. Basically, the protonation and

deprotonation of functional groups define the bio-adsorption mechanism [2,33]. It is important to comprehend that the pH of acidic nature has the maximum values of bio-adsorption. This is due to the fact that in the acidic zone, the overall charge on the bio-adsorbent for the removal can be positive or mainly positive, allowing negatively charged fluoride to attach to them readily. At a pH of 6, the optimum efficacy of 81.7% was found. Considerable adsorption performance was also accomplished at neutral pH equalling 7. However, the effectiveness of fluoride adsorption was slightly less than in the acidic stage (pH = 6). Fig. 6 shows that increasing the pH from 5 to 8 resulted in a 9% decrease in fluoride elimination.

3.4.2. Effect of initial fluoride concentration

0.4 g of the QOFWA was added up to several fluoride concentrations (2.5, 5.0, 7.5, 10, 12.5, and 15.0 mg L⁻¹) to evaluate the impact of initial fluoride concentrations on elimination efficiency. According to the findings (Fig. 7A), increasing the initial fluoride concentration (2.5–15 mg L⁻¹) led to a reduction in the fluoride removal rate from 85.6% to 56.1%. This was likely due to the limited amount of adsorbent material that was quickly depleted, like the initial

concentration of fluoride raised. This tendency has also been documented in the previous literature in the perspective of adsorption-based fluoride, phosphorous, and nitrate removal [2,16,20]. Furthermore, the research found that the quantity of fluoride adsorbed was firmly attributable to the rise in initial fluoride concentrations, which ranged from 0.54 to 2.21 mg g⁻¹ (Fig. 7B).

3.4.3. Effect of contact time

Another significant aspect addressed in this research is contact time. The observed rate of fluoride elimination was shown to be closely related to the contact time. Nevertheless, the linearity was not continuous since the percent fluoride elimination reached equilibrium. Contact duration changes outside this threshold revealed no directly proportional relationship (Fig. 8). Basically, three distinct stages were identified in the entire fluoride elimination mechanism. The very first stage was the initial peak part, during which the adsorbent absorbed fluoride ions substantially at both pH 6 and pH 7. The absorption was gradual during the second-stage. This showed that all active sites on the adsorbent surface had been consumed, as well as an indication that the equilibrium stage was approaching [6]. The third phase was basically the equilibrium phase, which was seen after 45 min. Only little additional absorption occurs during this stage, increasing the total removal of fluoride at pH 6 and 7 to just 84.3 % and 73.1%, respectively.

Table 2

Carbon-nitrogen-hydrogen analysis of raw olive fruit waste (OFW) and quaternized olive fruit and waste (QOFWA)

	OFW	QOFWA
Carbon (wt.%)	50.73	49.41
Hydrogen (wt.%)	5.63	6.35
Nitrogen (wt.%)	3.28	3.51
Oxygen (wt.%)	40.36	40.71
Sulfur (wt.%)	0.0017	0.0213

3.5. Langmuir and Freundlich isotherm analysis

To examine the applicability and performance of adsorption, the linearized version of Langmuir isotherm [Eqs. (1)–(3)] and Freundlich isotherm models [Eq. (4)] are employed [6,19].

The values of R_L were found to be less than 1 for all concentrations, indicating monolayer adsorption. Conversely,

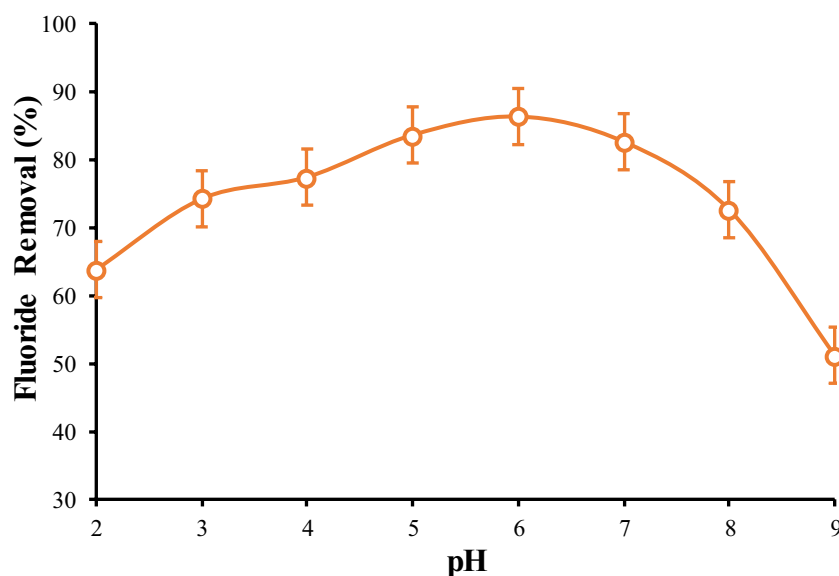


Fig. 6. The amount of fluoride adsorbed by QOFWA shown as the function of pH of aqueous solution (dosage: 4 g L⁻¹; temperature: 28°C).

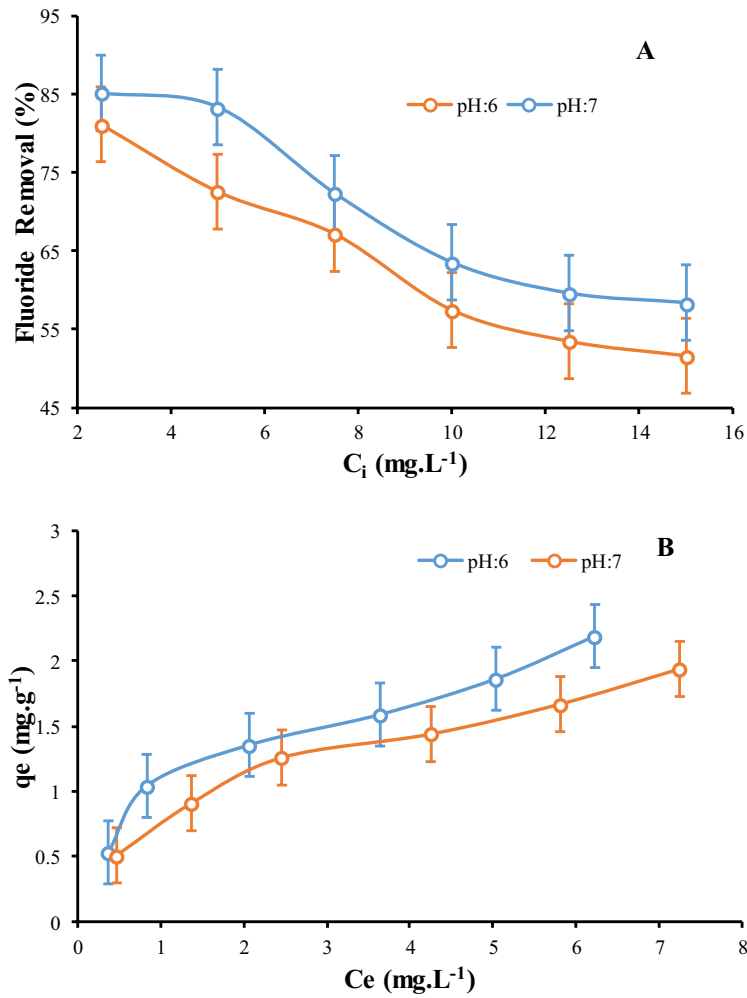


Fig. 7. (A) Influence of initial concentration on fluoride removal on QOFWA and (B) adsorption capacity (mg g⁻¹) at numerous initial concentrations of fluoride (dosage: 4 g L⁻¹; temperature: 28°C).

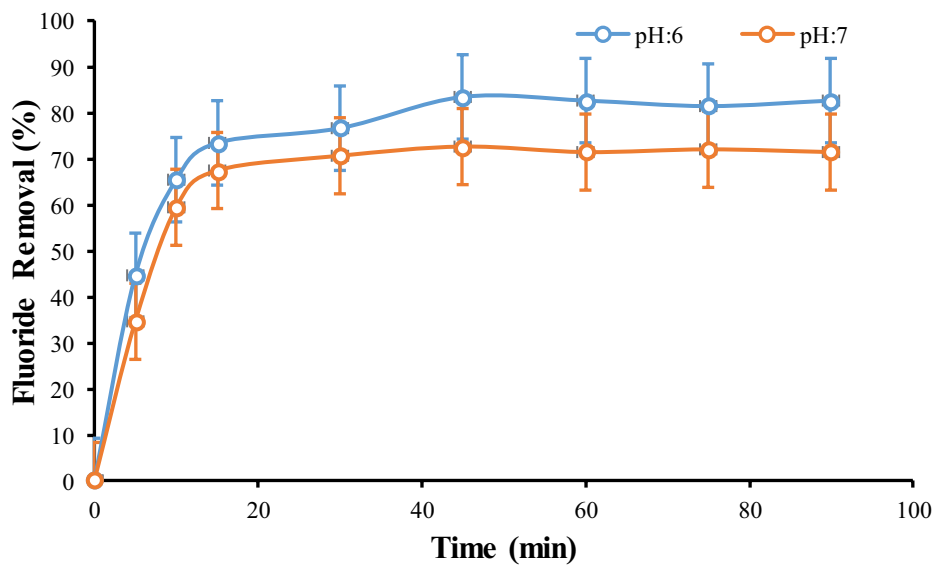


Fig. 8. Influence of contact time on fluoride removal on QOFWA at pH 6 and 7 (initial fluoride concentration: 2.5 mg L⁻¹; dosage: 4 g L⁻¹; temperature: 28°C).

the values obtained for K_f and n were found to range between 0 and 1, suggesting the restricted application of multilayer adsorption as well as physical adsorption owing to electrostatic attraction and repulsion. The R^2 values obtained for both the Langmuir and Freundlich models are above 0.9, that is, 0.985 and 0.954 (at pH 6) and 0.989 and 0.988 (at pH 7), respectively (Table 3). Considering the R^2 value, which indicates that monolayers outperform multilayers adsorption, the graph relating q_e and C_e (Fig. 9) perfectly matches this removal mechanism.

3.6. Adsorption kinetics

In order to examine the pseudo-first-order model and second-order model behavior, Eqs. (5) and (6) were used.

The constants K_1 and K_2 values were observed as 0.055 min^{-1} and $0.2904 \text{ g (mg min)}^{-1}$, respectively. R^2 factor is traditionally employed to conclude the best fit of the model, but it does not reflect errors in the curve [22]. To overcome this limitation, residual RMSE is calculated to observe the fitting of the curve because the lower is RMSE value, the better it will be fitting. It can be seen

Table 3

Observation of Langmuir and Freundlich parameters for fluoride adsorption on QOFWA

Isotherms	pH	Parameters	Fluoride adsorption
Langmuir	6	Q_0 (mg g^{-1})	2.350
		b (L mg^{-1})	0.809
		R^2	0.985
Freundlich	6	K_f (mg g^{-1})	0.943
		$1/n$	0.448
		N	2.234
Langmuir	7	Q_0 (mg g^{-1})	2.010
		b (L mg^{-1})	0.712
		R^2	0.989
Freundlich	7	K_f (mg g^{-1})	0.759
		$1/n$	0.478
		N	2.124
		R^2	0.988

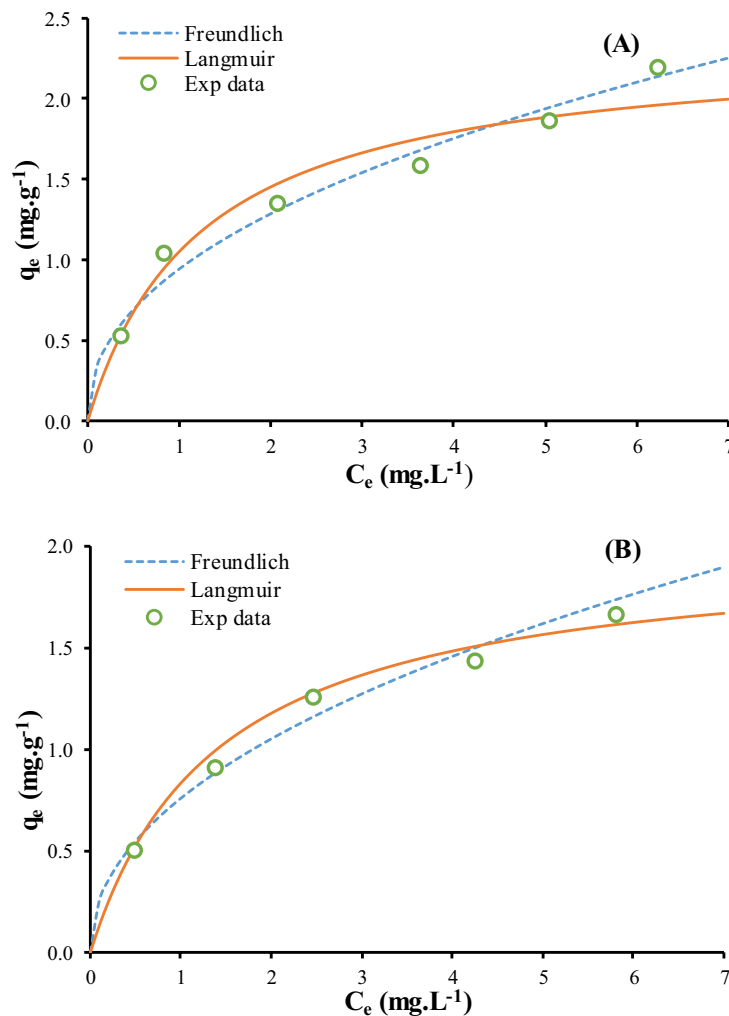


Fig. 9. Adsorption isotherms for fluoride removal on QOFWA as anticipated by the Langmuir and Freundlich models (A) pH 6 and (B) pH 7 (dosage: 4 g L^{-1} ; temperature: 28°C).

from Table 4 that the RMSE value for pseudo-second-order is less than pseudo-first-order as well as R^2 value was obtained as 0.902 for the pseudo-first-order and 0.999 for pseudo-second-order models. In the pseudo-second-order model, the q_e value was 1.073 mg g⁻¹. Resultantly, the chemisorption was observed dominating the adsorption of fluoride onto QOFWA. The pseudo-second-order model is shown to be a superior fit for this specific biosorption process (Figs. 10 and 11). Analogous findings have been stated in the previous studies for adsorbents made of palm oil waste and Sargassum sp. (seaweeds) [2,20,34].

3.7. Column study of fluoride sorption on QOFWA

3.7.1. Fixed-bed column study

Adsorption processes highly need the use of column studies. In the current study, initial column studies were done in the burette (11 mm diameter), aiming to examine the adsorption capacity, QOFWA dosage, and effectiveness for various particle sizes (0.25–0.5 mm).

A 7 mL s⁻¹ flow rate was used to study solutions with starting fluoride concentrations of 2.5 and 5 mg L⁻¹. At

10-min intervals, the effluent was collected. Fluoride’s breakthrough curve showed a similar tendency to nitrate’s sorption curve (Fig. 12). The column weakened in a shorter time while observing the initial concentration of 5 mg L⁻¹, but it was ignored as both curves were S-shaped, which is in accordance with earlier studies [16,35]. Amount of 3.14 to 5.15 mg g⁻¹ was determined to be the adsorption capacity at both doses, respectively (Fig. 12). As a result of fewer adsorbing sites being accessible at high concentrations, the column was predicted to be exhausted sooner.

3.7.2. Effect of size of QOFWA in fixed beds

An initial fluoride concentration of 2.5 mg L⁻¹ with a constant pH of 6 ± 0.2 was used to compute the impact of adsorbent size on reaction rate in a continuous flow fixed bed. The findings of the fixed bed column revealed that lowering the width or size of the QOFWA enhanced the saturation adsorption capacity for fluoride. It can be clearly seen in Table 5 that the fluoride-adsorption coefficient q_s was 1.47, 0.86, and 0.75 mg g⁻¹, corresponding to the size of QOFWA, that is, 0.125–0.25 mm (small), 0.25–0.5 mm (medium), and 0.5–1.0 mm (large), respectively. Compared

Table 4

Observations for pseudo-first-order and pseudo-second-order kinetic model parameters for fluoride adsorption onto QOFWA (pH: 6 and dose: 4 g L⁻¹)

C_i (mg L ⁻¹)	q_e (Exp) (mg g ⁻¹)	Kinetic models	Parameters	Value	H (mg g-min ⁻¹)
5	1.03	Pseudo-first-order model	K_1 (min ⁻¹)	0.0550	1.150
			q_e (mg g ⁻¹)	0.4915	
			R^2	0.902	
			RMSE	0.1430	
			K_2 (g mg-min ⁻¹)	0.2904	
		Pseudo-second-order model	q_e (mg g ⁻¹)	1.0728	
			R^2	0.999	
			RMSE	0.0537	

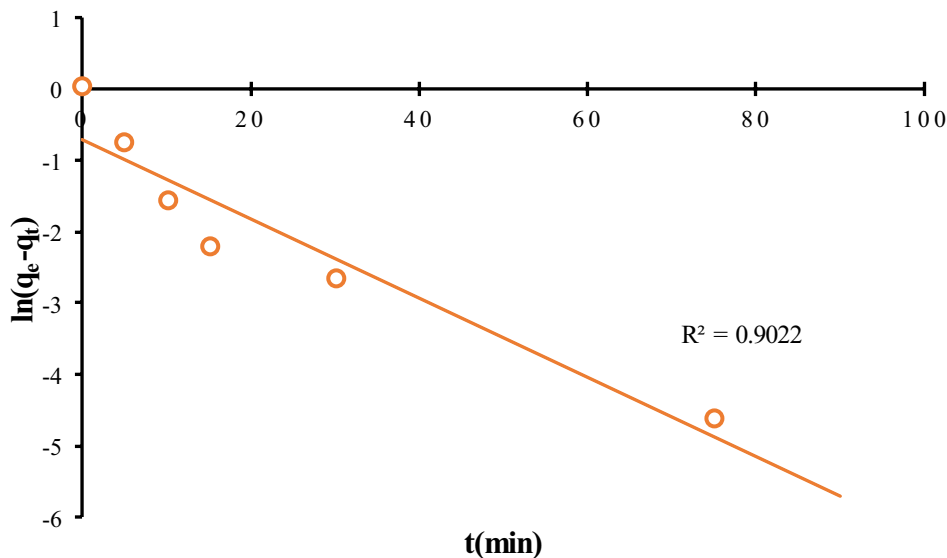


Fig. 10. Pseudo-first-order model-based kinetic rate of adsorption for fluoride onto QOFWA (pH: 6; dosages: 4 g L⁻¹).

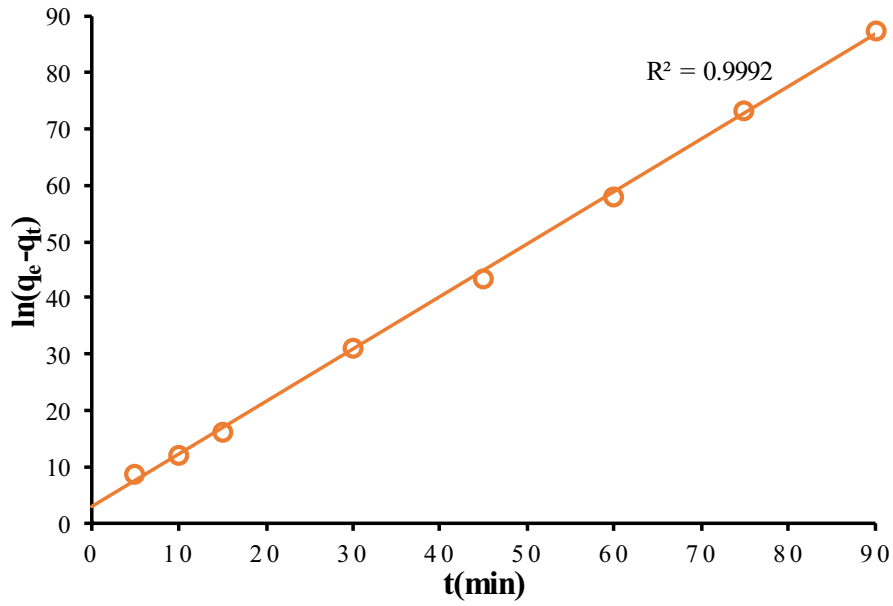


Fig. 11. Pseudo-second-order model based kinetic rate of adsorption for fluoride onto QOFWA (pH: 6; initial fluoride concentration: 5 mg L⁻¹; dosages: 4 g L⁻¹).

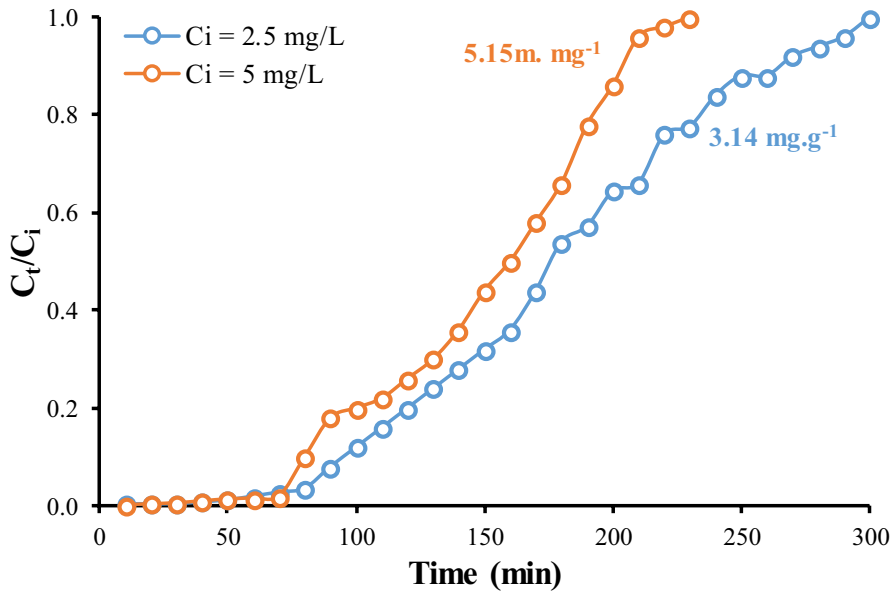


Fig. 12. Breakthrough curves for fluoride adsorption in fixed bed (initial fluoride concentration of 2.5 and 5 mg L⁻¹; flow rate of 7 mL min⁻¹; QOFWA dosage: 1 g; diameter of the column: 11 mm and pH: 6 ± 0.2).

Table 6

Observations for Adams–Bohart and Thomas model parameters at numerous flow rates in fixed-bed for fluoride sorption onto QOF-WA (initial fluoride cons.: 2.5 mg L⁻¹; pH: 6 ± 0.2)

Flow (mL min ⁻¹)	q_s (Exp.) (mg g ⁻¹)	EBCT (min)	Parameters of Adams–Bohart model			Parameters of Thomas model		
			K_{ab} (L mg min ⁻¹)	N_0 (mg L ⁻¹)	R^2	k_{th} (L mg min ⁻¹)	q_{th} (mg g ⁻¹)	R^2
7	1.47	1.25	0.00265	1401	0.907	0.00363	1.610	0.952
10	0.77	0.88	0.00710	658	0.901	0.01202	0.815	0.98
15	0.71	0.88	0.00810	655	0.902	0.01360	0.789	0.959

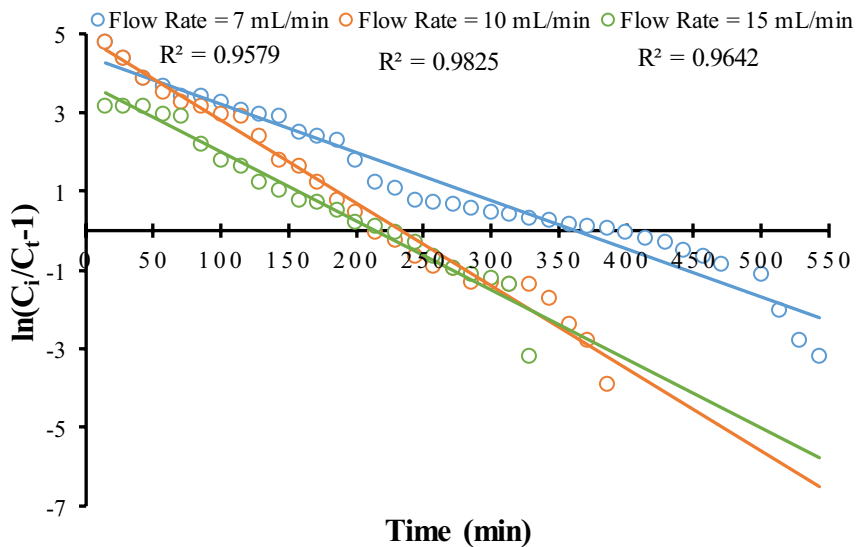


Fig. 13. Thomas regression coefficients for fluoride onto QOFWA at a flow rate of 7, 10, and 15 mL min⁻¹ (initial fluoride conc.: 2.5 mg L⁻¹; pH: 6 ± 0.2).

to a depth of 2.5, 3.0, and 3.5 cm, the mass of QOFWA with the size of 0.125–0.25 mm and 0.25–0.5 mm and 0.5–1 mm played a significant role. Other researchers have noted the same phenomenon in the case of the nitrate adsorption onto resins produced from wheat straw [25]. As shown in Fig. 13, the fluoride adsorption equilibrium concentration vs. time plot shows the creation of an S shape, which is essential to demonstrate the sorption in a column [16,24]. Furthermore, the breakthrough point (0.5 Co) arose earlier in the case of greater size particles compared to QOFWA particles of smaller size, as can be seen in Fig. 13.

3.8. Thomas and Adams–Bohart model analysis

The data were fitted in Thomas and Adams–Bohart models to evaluate the continuous flow columns design performance.

3.8.1. Thomas model

As the adsorbent size increased in the Thomas model, q_s and q_{th} dropped. While an increase in flow rate also led to an increase in " k_{th} " and a decrease in " q_s ". Based on the R^2 values recorded between 0.95 to 0.98 for varied flow rates and varying sizes of QOFWAs, the regression line functioned as a reasonable fit to the experimental data (Fig. 13). Since the adsorption process is not reliant on external and internal diffusions, Thomas's model proved a valuable tool [25,26]. Other scholars also reported a comparable result in the column adsorption process [23,24,36].

3.8.2. Adams–Bohart model

For fluoride adsorption, data were also fitted in the Adams–Bohart model, and all experimental designs had R^2 values nearer to one (Tables 5 and 6). For fluoride sorption, ' K_{ab} ' was determined to be 0.00265, 0.00710 and 0.0081 mg L⁻¹ at flow rates of 7, 10, and 15 mL min⁻¹, respectively (Table 6).

As the flow rate upsurges, the value of ' K_{ab} ' increases while the value of ' N_0 ' drops. By raising the flow rate, the kinetics of the entire system is regulated by external mass transfer in the first portion of column adsorption [25]. Despite the fact that the Adams–Bohart model provides a clear and all-inclusive method of measuring fluoride adsorption in the column, the validity of the model is restricted to the circumstances employed.

4. Conclusion

In this study, a novel QOFWA was effectively fabricated by the chemical modification of olive fruit waste. The resulting adsorbent demonstrated excellent fluoride adsorption in a comprehensive pH ranging from 3 to 9 and the highest fluoride adsorption ability at pH 6, equalling 83% removal with an adsorption capacity of 2.35 mg g⁻¹. Langmuir isotherm with $R^2 = 0.985$ was observed to be the best approach for the adsorption process, but Freundlich isotherm also established its successful adsorption ability. Along with the Langmuir, Freundlich isotherm also validated their adsorption performance and was determined to be a superior match for such adsorption mechanism. At the initial concentration (5 mg L⁻¹), adsorption kinetic analysis demonstrated that the high percentage of the elimination, that is, 83.4% and 72.6% at pH 6 and 7, respectively occurred rapidly in the first 15 min, accompanied through an equilibrium concentration at each pH values under consideration. The pseudo-second-order was observed better fit with $R^2 = 0.999$ and provided a removal capacity of 1.0728 mg L⁻¹ is almost equal to the experimental value of 1.03 mg L⁻¹.

SEM revealed dramatic modifications in surface structure as well as a reduced number of pores on the adsorbent. Furthermore, the existence of the amount of nitrogen on QOFWA was verified using EDX and CHN analysis. Because of the availability of adequate hemicellulose, the OFW was acceptable for the agro-based adsorbent. FT-IR studies found that CHMAC successfully reacted with mercerized

OFW, rendering its suitability for fluoride adsorption. Furthermore, the zeta potential and point of zero charge (pH_{PZC}) were 7.19 and 7.7, respectively.

Additionally, BET analysis verified the existence of macro and mesopores. The highest fluoride adsorption in a standardized column of diameter equal to 1.1 cm was determined to be 5.15 mg g⁻¹. The pseudo-second-order model ($R^2 = 0.999$) as well as Thomas and Adams–Bohart model models with $R^2 = 0.952$ and $R^2 = 0.907$, respectively, accurately represented the adsorption kinetics. The Thomas model demonstrated that the external mass transfer was accountable for regulating the reaction kinetics of the whole system. It is highly recommended to conduct further study on the evaluation of their application and usefulness in reducing heavy metals ions. In summary, it is expected that this innovative QOFWA would be a feasible technique for the efficient removal of fluoride.

Acknowledgment

The authors extend their appreciation to the Deanship of Scientific Research at Jouf University for funding this work through research grant No (DSR2020-06-3666).

References

- [1] T. Akafu, A. Chimdi, K. Gomoro, Removal of fluoride from drinking water by sorption using diatomite modified with aluminum hydroxide, *J. Anal. Methods Chem.*, 2019 (2019) 4831926, doi: 10.1155/2019/4831926.
- [2] M.T. Bashir, A. Salmiaton, M. Nourouzi, I. Azni, R. Harun, Fluoride removal by chemical modification of palm kernel shell-based adsorbent: a novel agricultural waste utilization approach, *Asian J. Microbiol. Biotechnol. Environ. Exp. Sci.*, 17 (2015) 533–542.
- [3] P. Pillai, S. Dharaskar, S. Pandian, H. Panchal, Overview of fluoride removal from water using separation techniques, *Environ. Technol. Innovation*, 21 (2020) 101246, doi: 10.1016/j.eti.2020.101246.
- [4] E.W. Wambu, W.O. Ambusso, C. Onindo, G.K. Muthakia, Review of fluoride removal from water by adsorption using soil adsorbents – an evaluation of the status, *J. Water Reuse Desal.*, 6 (2016) 1–29.
- [5] E. Annan, E. Nyankson, B. Agyei-Tuffour, S.K. Armah, G. Nkrumah-Buandoh, J.A.M. Hodasi, M. Oteng-Pepurah, Synthesis and characterization of modified kaolin-bentonite composites for enhanced fluoride removal from drinking water, *Adv. Mater. Sci. Eng.*, 2021 (2021) 6679422, doi: 10.1155/2021/6679422.
- [6] M.T. Bashir, A. Salmiaton, A. Idris, R. Harun, Kinetic and thermodynamic study of nitrate adsorption from aqueous solution by lignocellulose-based anion resins, *Desal. Water Treat.*, 62 (2017) 449–456.
- [7] A. Fadaei, Comparison of water defluoridation using different techniques, *Int. J. Chem. Eng.*, 2021 (2021) 2023895, doi: 10.1155/2021/2023895.
- [8] H.A. Ezzeldin, A. Apblett, G.L. Foutch, Synthesis and properties of anion exchangers derived from chloromethyl styrene codivinylbenzene and their use in water treatment, *Int. J. Polym. Sci.*, 2010 (2010) 684051, doi: 10.1155/2010/684051.
- [9] M. Zeng, Z. Fang, C. Xu, Novel method of preparing microporous membrane by selective dissolution of chitosan/polyethylene glycol blend membrane, *J. App. Polym. Sci.*, 91 (2004) 2840–2847.
- [10] M. Maduabuchi, Agricultural waste materials as a potential adsorbent for removal of heavy metals in wastewater, *Open Access J. Waste Manage. Xenobiotics*, 1 (2018) 000104.
- [11] L. Medouni-Haroune, F. Zaidi, S. Medouni-Adrar, M. Kecha, Olive pomace: from an olive mill waste to a resource, an overview of the new treatments, *J. Crit. Rev.*, 5 (2018) 1–6.
- [12] U.S. Orlando, A.U. Baes, W. Nishijima, M. Okada, Preparation of agricultural residue anion exchangers and its nitrate maximum adsorption capacity, *Chemosphere*, 48 (2002) 1041–1046.
- [13] Z. Muhammad, M.T. Bashir, A. Javid, F.A. Khan, S. Mujahid, Removal of Cu²⁺ from aqueous solution by activated carbon prepared from sawdust and nutshells, *Desal. Water Treat.*, 126 (2018) 171–180.
- [14] M.T. Bashir, Nitrate and Fluoride Adsorption from Aqueous Solution by Chemically Modified Palm Kernel Shells, University Putra Malaysia, 2016.
- [15] Y.S. Koay, I.S. Ahamad, M.M. Nourouzi, L.C. Abdullah, T.S.Y. Choong, Development of novel low-cost quaternized adsorbent from palm oil agriculture waste for reactive dye removal, *BioResources*, 9 (2014) 66–85.
- [16] X. Xing, B.-Y. Gao, Q.-Q. Zhong, Q.-Y. Yue, Q. Li, Sorption of nitrate onto amine-crosslinked wheat straw: characteristics, column sorption and desorption properties, *J. Hazard. Mater.*, 186 (2011) 206–211.
- [17] P. Goswami, R.S. Blackburn, H.M. El-Dessouky, J. Taylor, P. White, Effect of sodium hydroxide pre-treatment on the optical and structural properties of lyocell, *Eur. Polym. J.*, 45 (2009) 455–465.
- [18] A. Nega, Mercerization physical and chemical changes in cotton, 2011.
- [19] K.Y. Foo, B.H. Hameed, Insights into the modeling of adsorption isotherm systems, *Chem. Eng. J.*, 156 (2010) 2–10.
- [20] R. Nodehi, H. Shayesteh, A. Rahbar-Kelishami, Fe₃O₄@NiO core-shell magnetic nanoparticle for highly efficient removal of Alizarin red S anionic dye, *Int. J. Environ. Sci. Technol.*, (2021) 1–14, doi: 10.1007/s13762-021-03399-8.
- [21] H. Shayesteh, A. Rahbar-Kelishami, R. Norouzbeigi, Evaluation of natural and cationic surfactant modified pumice for congo red removal in batch mode: kinetic, equilibrium, and thermodynamic studies, *J. Mol. Liq.*, 221 (2016) 1–11, doi: 10.1016/j.molliq.2016.05.053.
- [22] A.-D. Noura, T.M. Abu-Sharar, Kinetics of fluoride adsorption onto native and Mg(OH)₂-amended limestone, *Appl. Water Sci.*, 11 (2021) 1–13, doi: 10.1007/s13201-021-01358-9.
- [23] M. Jahangiri-Rad, A. Jamshidi, M. Rafiee, R. Nabizadeh, Adsorption performance of packed bed column for nitrate removal using PAN-oxime-nano Fe₂O₃, *J. Environ. Health Sci. Eng.*, 12 (2014) 1–5.
- [24] R. Han, Y. Wang, X. Zhao, Y. Wang, F. Xie, J. Cheng, M. Tang, Adsorption of methylene blue by phoenix tree leaf powder in a fixed-bed column: experiments and prediction of breakthrough curves, *Desalination*, 245 (2009) 284–297.
- [25] X. Xu, B. Gao, X. Tan, X. Zhang, Q. Yue, Y. Wang, Q. Li, Nitrate adsorption by stratified wheat straw resin in lab-scale columns, *Chem. Eng. J.*, 226 (2013) 1–6.
- [26] R. Han, Y. Wang, W. Zou, Y. Wang, J. Shi, Comparison of linear and nonlinear analysis in estimating the Thomas model parameters for methylene blue adsorption onto natural zeolite in fixed-bed column, *J. Hazard. Mater.*, 145 (2007) 331–335.
- [27] D. Prahas, Y. Kartika, N. Indraswati, S. Ismadji, The use of activated carbon prepared from jackfruit (*Artocarpus heterophyllus*) peel waste for methylene blue removal, *J. Environ. Protect. Sci.*, 2 (2008) 1–10.
- [28] C.T. Chiou, J. Cheng, W.-N. Hung, B. Chen, T.-F. Lin, Resolution of adsorption and partition components of organic compounds on black carbons, *Environ. Sci. Technol.*, 49 (2015) 9116–9123.
- [29] N. Mokaloba, R. Batane, The effects of mercerization and acetylation treatments on the properties of sisal fiber and its interfacial adhesion characteristics on polypropylene, *Int. J. Eng. Sci. Technol.*, 6 (2014) 83–97.
- [30] P. Koochi, A. Rahbar-Kelishami, H. Shayesteh, Efficient removal of congo red dye using Fe₃O₄/NiO nanocomposite: synthesis and characterization, *Environ. Technol. Innovation*, 23 (2021) 101559.
- [31] N.A. Medellin-Castillo, R. Leyva-Ramos, E. Padilla-Ortega, R. Ocampo Perez, J. Flores-Cano, M.S. Berber-Mendoza,

- Adsorption capacity of bone char for removing fluoride from water solution. Role of hydroxyapatite content, adsorption mechanism and competing anions, *J. Ind. Eng. Chem.*, 20 (2014) 4014–4021.
- [32] S. Jenish, P.A. Methodis, Fluoride removal from drinking water using used tea leaves as adsorbent, *Asian J. Chem.*, 23 (2011) 2889–2892.
- [33] F. Amin, F.N. Talpur, A. Balouch, M.A. Surhio, M.A. Bhutto, Biosorption of fluoride from aqueous solution by white-rot fungus *Pleurotus eryngii* ATCC 90888, *Environ. Nanotechnol. Monit. Manage.*, 3 (2015) 30–37.
- [34] J. Jiménez-Becerril, M. Solache-Ríos, I. García-Sosa, Fluoride removal from aqueous solutions by boehmite, *Water Air Soil Pollut.*, 223 (2012) 1073–1078.
- [35] W. Zou, L. Zhao, L. Zhu, Adsorption of uranium(VI) by grapefruit peel in a fixed-bed column: experiments and prediction of breakthrough curves, *J. Radioanal. Nucl. Chem.*, 295 (2013) 717–727.
- [36] S. Chen, Q. Yue, B. Gao, Q. Li, X. Xu, K. Fu, Adsorption of hexavalent chromium from aqueous solution by modified corn stalk: a fixed-bed column study, *Bioresour. Technol.*, 113 (2012) 114–120.